Metamaterials for Enhanced Polarization Conversion in Plasmonic Excitation

Liang Feng,[†] Amit Mizrahi, Steve Zamek, Zhaowei Liu,* Vitaliy Lomakin, and Yeshaiahu Fainman*

Department of Electrical and Computer Engineering, University of California, San Diego, La Jolla, California 92093, United States. [†] Department of Electrical Engineering, California Institute of Technology, Pasadena, California 91125, United States

Plasmonics has been making break-through improvements in the field of nanophotonics due to its ability of extreme field confinement,[1,2] finding myriad applications in bioimaging,[3−6] biosensing,[7] data storage,[8] photovoltaics,[9] light emission sources,[10,11] and compact on-chip device integration.[12−15] Because of the intrinsic transverse magnetic (TM) nature of plasmonic fields, however, surface plasmons (SPs) efficient excitation is strongly constrained to TM polarized incidence, so that for unpolarized light, 50% of the energy that is transverse electric (TE) polarized cannot be utilized. Designer plasmons, also called *spoof* plasmons, refer to surface-plasmon-like waves on textured metal surfaces, which can be supported in periodic structures that may be made of perfect conductors,[16−22] for instance. Designer plasmons rely on either evanescent or propagating modes inside the textured surface, with significant property variations for the two cases.[16,17] The latter offers particular flexibility and can lead to surface modes with a very large wavevector. The existence of such plasmons is attributed to the fact that the textured surface can be viewed as imposing an effective surface impedance, which can be artificially engineered by the structure geometrical parameters, such as the periodicity, duty cycle, and thickness of the metallic features. In the terahertz and microwave regimes, designer plasmonic metamaterials have been constructed to realize waveguiding and focusing,[20,21] as well as to engineer the slow wave characteristics of the guided microwave.[22] However, similarly to natural surface plasmons (SPs) on metallic surfaces in the optical regime, such designer plasmons are also intrinsically TM polarized, which makes the efficient manipulation of TE fields by such structures challenging, as only TM excitation has been demonstrated so far.[16−22]

ABSTRACT Surface plasmons efficient excitation is typically expected to be strongly constrained to transverse magnetic (TM) polarized incidence, as demonstrated so far, due to its intrinsic TM polarization. We report a designer plasmonic metamaterial that is engineered in a deep subwavelength scale in visible optical frequencies to overcome this fundamental limitation, and allows transverse electric (TE) polarized incidence to be strongly coupled to surface plasmons. The experimental verification, which is consistent with the analytical and numerical models, demonstrates this enhanced TE-to-plasmon coupling with efficiency close to 100%, which is far from what is possible through naturally available materials. This discovery will help to efficiently utilize the energy fallen into TE polarization and drastically increase overall excitation efficiency of future plasmonic devices.

KEYWORDS: pure TE-to-plasmon coupling · designer (*spoof*) plasmons · metamaterial · polarization conversion · hybrid Bloch modes

Textured metallic surfaces with designer plasmons in the optical regime have a high potential to result in a number of unique phenomena due to possible interplay between the plasmonic properties of metals and properties derived from structural features of the textured surface. We show below that the complexity of the resulting electromagnetic phenomena may provide us with great freedom to tailor the propogation of SPs as well as to design a pure TE-driven SP, complementing the so far demonstrated TM-polarized excitation. Here, "pure TE" means the polarization of the incident light is transverse to both SPs and the plane-of-incidence, to distinguish with diffraction gratings where "TE" is defined only with respect to the plane-of-incidence but not to SPs.[23] The importance of the pure TE definition lies in the fact that SPs are inherently TM with respect to their direction of propagation, so that to overcome this fundamental limitation, one must consider TE with respect to the SP direction as well, that is, a polarization that is completely orthogonal to that of the excited propagating SPs. In this study, we present for the first time an optical designer plasmonic metamaterial,[17]
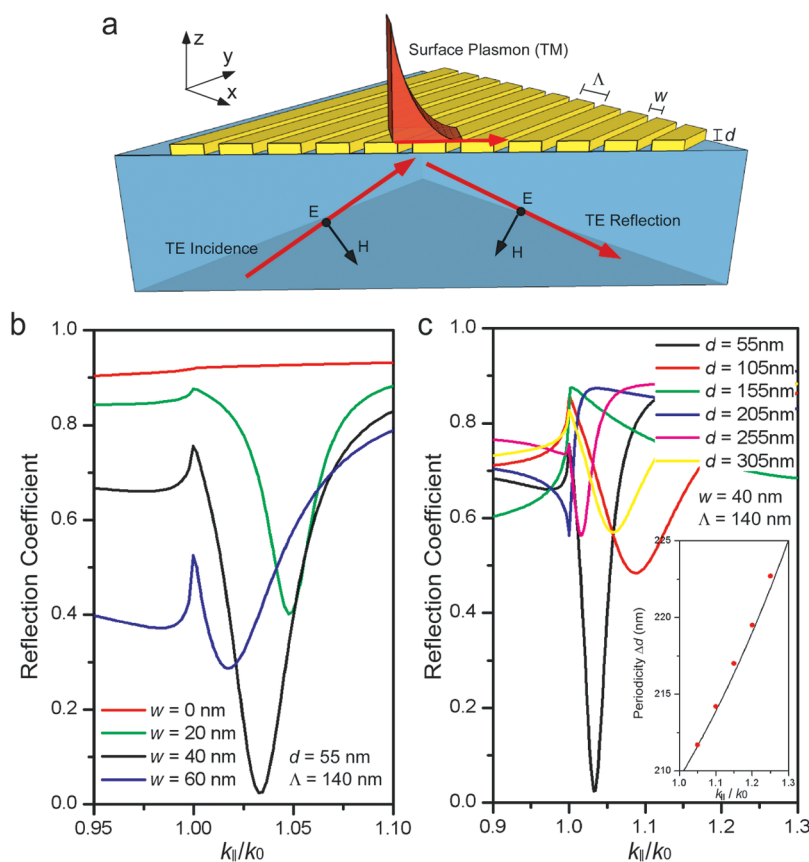
Figure 1. Design of the plasmonic metamaterial. (a) Schematic of enhanced pure TE-to-plasmon coupling with the designer plasmonic metamaterial. Pure TE-polarized plane wave incidents from a glass substrate ($n = 1.5$) with the incident plane as the diagonal cross-section of the metamaterial slab and excites SPs at the air/metamaterial interface. (b) Simulated reflection spectra at 640 nm with the fixed thickness $d = 55$ nm and period $\Lambda = 140$ nm, for different air slit widths w. (c) Simulated reflection spectra at 640 nm with the fixed period $\Lambda = 140$ nm and air slit width $w = 40$ nm, for different slab thicknesses d. The inset shows the periodicity of the mode in thickness at different eigen-vectors of surface modes retrieved from mode analysis (black) and simulations (red), exhibiting typical features of designer SPs.

which combines plasmonic properties of metals in optics and properties of designer textured surfaces typically observed in microwave structures. The metamaterial introduced here supports designer SPs in remarkable frequency and wavevector ranges, including surface modes with a large effective index that efficiently couple to the pure TE polarized light.

RESULTS AND DISCUSSION

Engineering of the Visible-Frequency Designer (*Spoof*) Plasmonic Metamaterial. The presented designer plasmonic metamaterial consists of Au stripes periodically arranged in a deep subwavelength scale as shown in Figure 1a. Because of the deep subwavelength nature of the structure, the diffraction orders are evanescent and therefore the metamaterial shows a uniform optical response without involving any diffraction, in stark contrast to previously investigated conventional diffraction gratings with feature sizes on the order of the wavelength[1,2,7,14,23] where the diffraction plays dominant roles. So far similar metamaterials were analyzed only in two-dimensional (2D) configurations, and for the terahertz regime.[17,20,22] In contrast, in this study we

operate in the optical regime, and consider an incident wave with a nonzero azimuth and elevation angles, requiring a fully three-dimensional (3D) analysis and physical understanding. The domain between the top and bottom faces of the metamaterial acts as an array of coupled metal—insulator—metal (MIM) plasmonic transmission lines,[24] supporting plasmonic Bloch modes guided in the vertical direction. Because of the 3D nature of the problem, the modes are hybrid, consisting of both TM and TE polarized components. A combination of the modes guided in the upward and downward directions is required to satisfy the boundary conditions on the top and bottom faces of the metamaterial. Because of the extremely thin width of the metallic stripes that is on the order of the skin depth, the plasmonic modes in different MIM transmission lines are not independent and the introduced periodic potential makes a collectively oscillating plasmonic Bloch modes in the periodic array of transmission lines. In particular, the hybrid nature of the supported Bloch mode can provide modes overlap and bridge a pure TE incident wave and excited SP waves, thereby creating enhanced pure TE-to-plasmon coupling in the designer plasmonic metamaterial.

Computer simulations were performed to validate the proposed pure TE-to-plasmon coupling and to optimize the geometry parameters of the designer plasmonic metamaterial. For the simulations and experiments we choose to use visible wavelengths varying from 540 to 680 nm with a focus on a detailed study at the wavelength of 640 nm. Rigorous coupled wave analysis (RCWA),[25] that was developed for studying periodic structures, was employed to calculate reflection coefficients for a pure TE polarized plane wave incident from a high-index substrate ($n = 1.5$) side. The corresponding dielectric constants of Au are extracted from data in ref 26. The geometry was optimized to achieve a minimum reflection coefficient which corresponds to maximum excitation efficiency of SPs. We consider the case where the incident wavevector (K_x, K_y, K_z), has an in-plane projection along the diagonal, such that $K_x = K_y = k_\parallel/\sqrt{2}$, and $k_\parallel$ is the parallel wavevector. At the resonant condition where minimum reflection is achieved and SPs are well excited, the parallel wavevector $k_\parallel$ corresponds to the wavevector of the SPs, k_{sp}. Figure 1 panels b and c show the reflection coefficient as a function of the parallel wavevector of the incident wave for different air slit widths and different slab thicknesses, respectively. We determined that the optimal geometry has a period of $\Lambda = 140$ nm, slit width of $w = 40$ nm, and slab thickness of $d = 55$ nm. The reflection coefficient at the dip is almost vanishing so that a nearly perfect (100%) pure TE-to-plasmon coupling efficiency was achieved.

To gain insight into the coupling mechanism, we investigate analytically the electromagnetic Bloch eigenmodes propagating in the positive and negative z directions inside the metamaterial slab. As explained above, these modes are hybrid, but since the slab is a periodic layered medium in the x direction, the modes are either TM or TE with respect to that direction, denoted by TM_x and TE_x, respectively (see Methods). The complex wavevectors β_z in the z direction vary as a function of the parallel in-plane wavevector $k_\parallel = k_{sp} = (K_x^2 + K_y^2)^{1/2}$ at the resonant condition where SPs are excited. Values of β_z corresponding to different eigenmodes are given in Table 1 for the two lowest modes (TM_x and TE_x) for different in-plane wavvectors. The fundamental mode is TM_x, and it has a dominant real part of β_z, such that it is mainly propagating. The higher order TM_x modes as well as all TE_x modes are evanescent with a dominant imaginary part of β_z. Therefore, for large thicknesses, the fundamental mode is almost solely responsible for the power transfer above the slab, satisfying the boundary conditions and leading to the surface mode on the metamaterial surface. So the angle of the dip viewed in reflection as a function of the slab thickness is thus expected to be periodic with a period of half the fundamental TM_x mode's effective wavelength $\Delta d = \lambda k_0/2\mathrm{Re}\{\beta_z\}$, as shown in Figure 1c.

TABLE 1. Complex Wavevectors β_z Normalized by k_0 in the z Direction of the Two Lowest Modes (TM_x and TE_x) with Different Parallel in-Plane Wavevectors k_{sp} of the Designer SP, Calculated at a Wavelength of 640 nm

mode	Re (k_{sp}) = 1.05k_0	Re (k_{sp}) = 1.1k_0	Re (k_{sp}) = 1.15k_0	Re (k_{sp}) = 1.2k_0	Re (k_{sp}) = 1.25k_0
TM_x	1.512−0.046j	1.496−0.047j	1.479−0.048j	1.461−0.049j	1.442−0.051j
TE_x	0.120−2.616j	0.119−2.634j	0.118−2.654j	0.117−2.674j	0.115−2.695j

In other words, when increasing the thickness of the metamaterial by Δd, the excited SP modes will have the same in-plane wavevector. This is shown in the inset of Figure 1c, where this quantity is calculated according to the values of β_z and compared with the exact period as a function of thickness variation. This periodic behavior is typical of designer SPs,[17] and distinguishes them from conventional SPs on a plane metal.

It is worth reemphasizing that the polarization conversion in our structure is enabled by the 3D field variation of the hybrid Bloch modes supported by the metallic slits. Different hybrid modes get strongly coupled with each other while propagating inside the metamaterial slab, which is significantly distinguished from the common 2D cases where TE and TM modes are decoupled.[27,28] At the resonance point, the supported hybrid modes are propagating back and forth within the slab in a similar way to a Fabry−Perot configuration, as seen from Figure 1c. The excited resonant hybrid modes strongly enhance the efficiency of the polarization conversion, which results in a complete conversion within a 55 nm thin slab, though the thickness is only equivalent to 0.13 effective wavelengths of the fundamental TM_x mode. However, it typically requires 0.5 effective wavelengths to form a half wave plate phase change to support such complete polarization conversion.[29,30]

Characterization of the Plasmonic Metamaterial. To fabricate the designed optimized subwavelength structure, we used focused-ion-beam (FIB) milling of an Au film on a glass substrate. The scanning electron microscopy (SEM) micrograph of the fabricated structure is shown in Figure 2. The excited designer SP modes in the fabricated metamaterial are characterized in reciprocal space by directly analyzing reflection images of the index ellipsoids of the SPs in the k space as shown in Figure 2a (see details in ref 31). These images are obtained from the glass substrate side of the sample inserted in an oil immersion microscope objective (MO) with a high numerical aperture (NA = 1.4). A converging polarized spherical wave is used as an illumination function to code a wide-band angular spectrum of the illumination. The size of the obtained reflection image at the back focal plane is limited by the NA of our MO that corresponds to a free space wavevector of 1.4k_0. Note that the central dark ring in
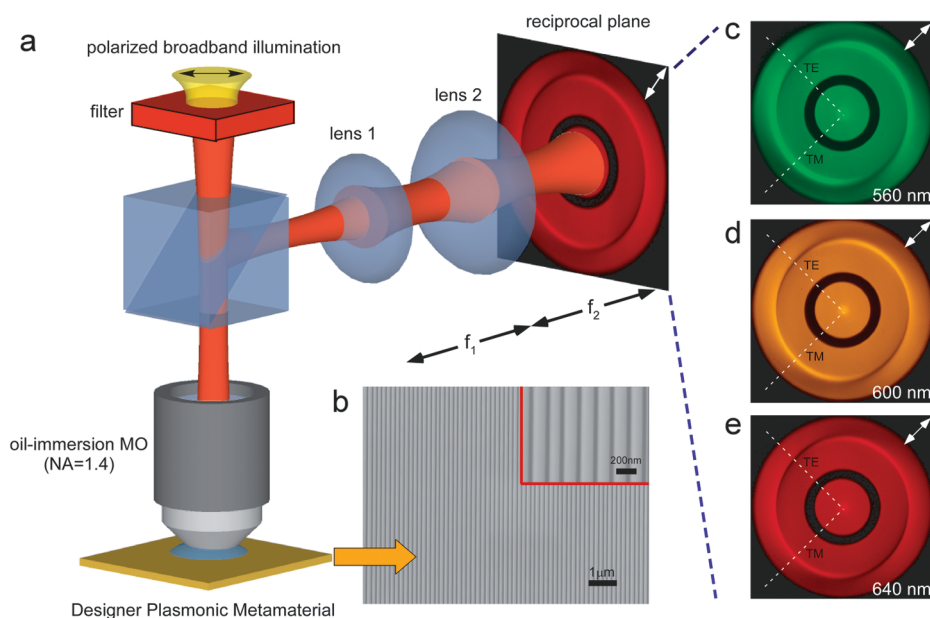
Figure 2. Experimental results of designer SPs. (a) Measurement configuration that can directly capture the index ellipsoids by imaging the reflection in reciprocal space. (b) SEM micrographs of the fabricated metamaterial. (c) Measured index ellipsoid at 560 nm. (d) Measured index ellipsoid at 600 nm. (e) Measured index ellipsoid at 640 nm.

Figure 2 panels c—e (*i.e.*, image of the phase ring inside the phase contrast MO) obscures some information, but the information of interest in our study lies at larger wavevectors. The dark tails (reflection dips) in the reflected images correspond to excitation of the designer SPs, in a similar manner to excitation of SPs at the Kretschmann configuration, and represent information about their index ellipsoids. These measurements are performed as a function of optical wavelength using a white light source in combination with a series of 10 nm bandpass interference filters in the spectral range of interest, that is, from 540 to 680 nm as shown in Figures 2c—e, for wavelengths of 560, 600, and 640 nm, respectively. The polarizer is oriented at an angle of 45° with respect to the *x* direction. Therefore TM components are lying in the plane of 45°, while the pure TE field is in the plane of −45°. Thus the diagonals contain information about pure TE and TM components while the remainder of the space represents linear combinations of TE and TM incident waves. Since TE and TM are orthogonal, all the necessary information lies in the diagonals.

Enhanced Pure TE-to-Plasmon Coupling. The numerically simulated and experimentally measured index ellipsoids of the designer plasmon modes in reciprocal space is shown in Figure 3 panels a and b, respectively, for a wavelength of about 640 nm. The detailed reflection spectra for pure TE and TM incidence have been extracted from the perpendicular (−45°) and parallel (45°) to the polarization planes, respectively, showing a good agreement between the experimental data and the simulation, as seen in Figure 3c. The slight discrepancy in the reflection spectrum observed around $k_\parallel = k_0$ for the TE polarization may come from the

imperfect fabrication during the FIB etching. The enhanced pure TE-to-plasmon coupling is observed as a sharp dip that occurs where its incident parallel wavevector satisfies the phase matching condition to excite the designer SPs. However, in contrast to excitation of conventional SPs, there is no pronounced dip in the reflectivity of TM polarization, indicating that surface waves are not excited.

The inherent nature of the surface mode supported by this enhanced pure TE-to-plasmon coupling has been further investigated using finite element method (FEM) simulations, showing strong field confinement on the surface and exponentially decaying fields into the air, associated with this mode, as seen in Figure 4. Remarkably, although the polarization of the incident field is pure TE, the excited surface mode is almost entirely TM-polarized, as E_z and the magnetic field transverse to the direction of propagation $H_\perp$ are strongly dominant. This polarization conversion from pure TE incidence to TM SPs is with about 98% efficiency. The diagonal orientated air slits act as a series of coupled transmission lines that efficiently transfer the power through the hybrid plasmonic modes inside the metamaterial slab. These excited hybrid modes possess different propagating characteristics and the resulting interference between them in each electric field component leads to strong polarization conversion. Specifically for the pure TE, the E_x component strongly overlaps with the fundamental TM_x mode, and the E_y is required to provide a diagonal $k_\parallel$ that would have an *x* component, so that E_x is rotated around the corner of the slits to become the E_z of the excited SPs. In addition to the fundamental difference in physics compared to coupling TE waves to SPs using
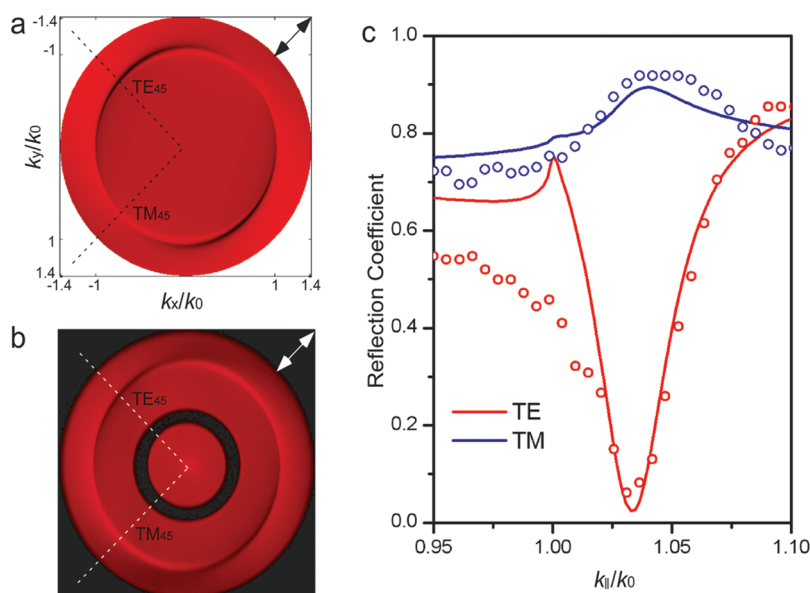
Figure 3. Enhanced pure TE-to-plasmon coupling at 640 nm. (a) Simulated index ellipsoid of the excited surface mode in a representation of reflected power distribution in reciprocal space. (b) Experimental imaging of reflection from the metamaterial in reciprocal space. (c) Detailed reflection spectra retrieved from panels a and b as TM (blue) is parallel and pure TE (red) is perpendicular to the incident polarization. Solid curves and hollow circles represent the results from simulation and experiment, respectively.
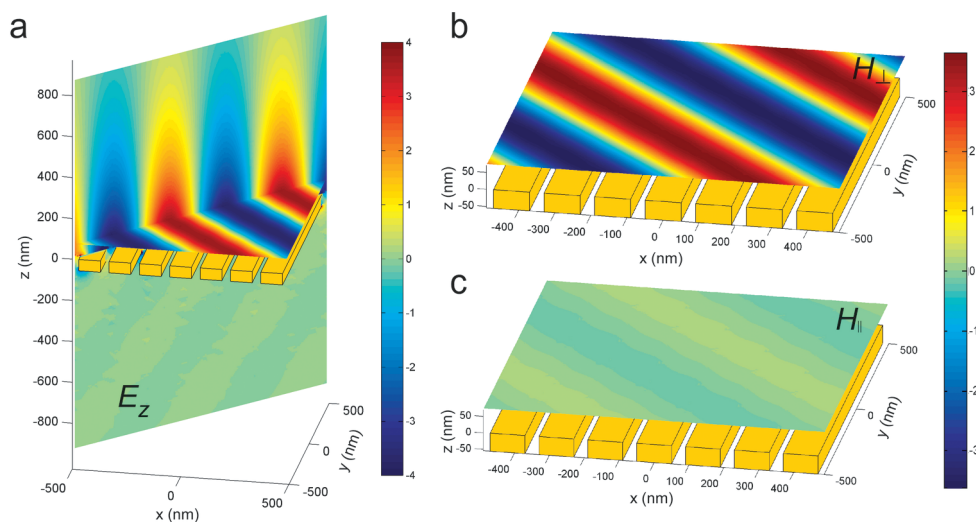

Figure 4. FEM simulations of the excited surface mode. (a) Field distributions of E_z in the diagonal cross-section and x-y plane, respectively. (b) Field mapping of the in-plane magnetic field component transverse to k_{sp}, $H_\perp$ (TM component). (c) Field mapping of the in-plane magnetic field component parallel to k_{sp}, $H_\parallel$ (TE component), showing TM characteristics associated with designer SPs.

a 2D metallic nanohole array,[32] the presented pure TE-to-SP coupling also shows a much higher efficiency (98% *vs* 10−20% depending on the design of the nanohole arrays).

Figure 5 shows the dispersion relation of the designer SPs. The experimentally measured wavevectors from Figure 2 at different wavelengths are compared with the wavevectors obtained by numerical simulations, which are the locations of the dips in the simulated reflection spectra of pure TE incidence. Similarly to conventional SPs, the designer SPs are associated with larger wavevectors at shorter wavelengths,

asymptotically approaching the effective surface plasma frequency. In the range of interest, the experimental and theoretical results are found to be in very good agreement, manifesting a broadband enhanced pure TE-to-plasmon coupling of our designer plasmonic metamaterial. Although the optimum design was performed for the wavelength of 640 nm, high coupling efficiencies are obtained in a range of over 100 nm (*i.e.*, 70% at 560 nm and 90% at 660 nm), showing broadband operation. From RCWA simulations, we extracted the effective wavevectors of SPs at different wavelengths: at 680 nm, $k_{sp} = k_0(1.015 − j0.007)$; at 640 nm,
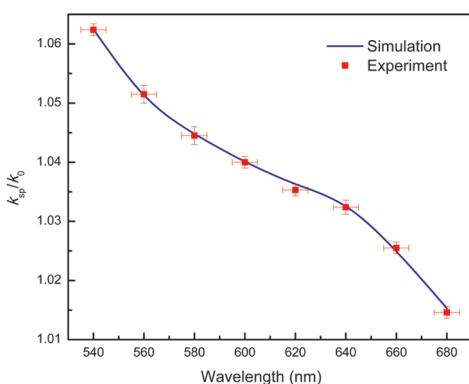
Figure 5. Dispersion relation of excited designer SP waves at the air/metamaterial interface. Solid curve and square markers correspond to data retrieved from numerical simulations and experimental measurements, respectively. For the experimental data, the error-bar in wavelengths indicates the bandwidth (10 nm) of the bandpass filters used in the experimental measurement.

$k_{sp} = k_0(1.033 - j0.013)$; at 560 nm, $k_{sp} = k_0(1.051 - j0.029)$. The corresponding propagation lengths of SPs are 7.7, 3.9, and 1.5 μm at 680, 640, and 560 nm, respectively. For comparison, at a wavelength of 640 nm the propagation length on a uniform Au film on a glass prism is 4.0 μm, such that the propagation length on the metamaterial is shorter by only about 3%, demonstrating almost the same excitation efficiency and inherent surface mode characteristics. Therefore the presented metamaterial may be considered complementary to the conventional SPs for TE polarization. It is thus expected that light absorption efficiency for unpolarized light may be drastically improved with a device that can incorporate charac-

teristics of both pure TE-to-SPs in our metamaterial and conventional TM SPs on plane metals.

CONCLUSIONS

The presented optical designer plasmonic metamaterial overcomes the inherent limitation of the TM-polarization nature of the SPs and supports highly efficient broadband pure TE-to-plasmon coupling. Our results are promising for improving the overall plasmonic excitation efficiency in a wide range of applications, including plasmon-assisted photovoltaics and on-chip plasmonic circuits. While the investigated geometry in this work varies only in two dimensions, the optical fields vary in all three dimensions. Thus the plasmonic modes that facilitate the demonstrated phenomena become hybrid, in contrast to previously investigated 2D problems. Engineered in the 3D deep subwavelength "artificial molecules" of metamaterials, the plasmonic hybrid modes open a door to allow sophisticated nanometric linear and circular polarization mixing, as well as conversion and manipulation of optical guided and free space waves. Further complication of the geometry of designer (*spoof*) plasmon metamaterials can offer significant possibilities for creating more counterintuitive optical responses, for example, using complementary split ring resonators to introduce magneto- and electro-inductive couplings between adjacent unit cells.[33,34] As a result, better confinement of the excited surface modes can be expected, which may lead to more efficient polarization conversion. This concept may be further extended to 3D layered structures[35,36] by engineering the vertical connectivity between different layers, providing flexibilities in the design of novel nanophotonic structures.

METHODS

Analysis of Bloch Modes Propagating Inside the Metamaterial. The dispersion relation for the Bloch modes that propagate inside the metamaterial slab is obtained by imposing the boundary conditions at the interfaces, as well as the Floquet theorem with a periodic phase corresponding to the incident wave vector (K_x, K_y), which, for the excitation along the diagonal, is given by $K_x = K_y = (\sqrt{2}/2)k_\parallel$. The dispersion relation is then given by

$$\frac{(Z_a + Z_m)^2}{4Z_a Z_m} \cos[k_{x,a}w + k_{x,m}(\Lambda - w)] - \frac{(Z_a - Z_m)^2}{4Z_a Z_m} \cos[k_{x,a}w$$

$$- k_{x,m}(\Lambda - w)] = \cos(K_x \Lambda)$$

where the wavevectors in the x direction are $k_{x,i} = (k_0^2 \varepsilon_i - K_y^2 - \beta_z^2)^{1/2}$, the impedances are $Z_i = \eta_0 k_{x,i}/(k_0 \varepsilon_i)$ for TM_x modes, and $Z_i = \eta_0 k_0/k_{x,i}$ for TE_x modes, ε_i are the permittivities in each region, and $i = $ a, m for the air and metal, respectively; η_0 is the vacuum impedance. The dispersion relation can then be solved to obtain the complex β_z. The first TM_x mode is a TEM-like mode in the slits. The second mode is a TE_x evanescent-like mode.

REFERENCES AND NOTES

1. Barnes, W. L.; Dereux, A.; Ebbesen, T. W. Surface Plasmon Subwavelength Optics. *Nature* **2003**, *424*, 824–830.
2. Ebbesen, T. W.; Lezec, H. J.; Ghaemi, H. F.; Thio, T.; Wolff, P. A. Extraordinary Optical Transmission through Subwavelength Hole Arrays. *Nature* **1998**, *391*, 667–669.
3. Pendry, J. R. Negative Refraction Makes a Perfect Lens. *Phys. Rev. Lett.* **2000**, *85*, 3966–3969.
4. Fang, N.; Lee, H.; Sun, C.; Zhang, X. Sub-diffraction-limited Optical Imaging with a Silver Superlens. *Science* **2005**, *308*, 534–537.
5. Liu, Z.; Lee, H.; Xiong, Y.; Sun, C.; Zhang, X. Far-Field Optical Hyperlens Magnifying Sub-diffraction-limited Objects. *Science* **2007**, *315*, 1686.
6. Kawata, S.; Non, A.; Verma, P. Subwavelength Colour Imaging with a Metallic Nanolens. *Nat. Photon.* **2008**, *2*, 438–442.
7. Pang, L.; Hwang, G.; Slutsky, B.; Fainman, Y. Spectral Sensitivity of Two-Dimensional Nanohole Array Surface Plasmon Polariton Resonance Sensor. *Appl. Phys. Lett.* **2007**, *91*, 123112.
8. Srituravanich, W.; Pan, L; Wang, Y; Sun, C; Bogy, D. B.; Zhang, X. Flying Plasmonic Lens in the Near Field for High-Speed Nanolithography. *Nat. Nanotechnol.* **2008**, *3*, 733–737.
9. Cao, L; White, J. S.; Park, J. S.; Schuller, J. A.; Clemens, B. M.; Brongersma, M. L. Engineering Light Absorption in

Semiconductor Nanowire Devices. *Nat. Mater.* **2009**, *8*, 643–647.

10. Zheludev, N. I.; Prosvirnin, S. L.; Papasimakis, N.; Fedotov, V. A. Lasing Spaser. *Nat. Photon.* **2008**, *2*, 351–354.

11. Oulton, R. F.; Sorger, V. J.; Zentgraf, T.; Ma, R. M.; Gladden, C.; Dai, L.; Bartal, G; Zhang, X. Plasmon Lasers at Deep Subwavelength Scale. *Nature* **2009**, *461*, 629–632.

12. Koller, D. M.; Hohenau, A.; Ditlbacher, H.; Galler, N.; Aussenegg, F. R.; Leitner, A.; List, E. J. W.; Krenn, J. R. Organic Plasmon Emitting Diode. *Nat. Photon.* **2008**, *2*, 684–687.

13. Pacifici, D.; Lezec, H. J.; Atwater, H. A. All-Optical Modulation by Plasmonic Excitation of CdSe Quantum Dots. *Nat. Photon.* **2007**, *1*, 402–406.

14. Yu, N.; Fan, J.; Wang, Q. J.; Pflugl, C.; Diehl, L.; Edamura, T.; Yamanishi, M.; Kan, H.; Capasso, F. Small-Divergence Semiconductor Lasers by Plasmonic Collimation. *Nat. Photon.* **2008**, *2*, 564–570.

15. Cai, W.; Chettiar, U. K.; Kildishev, A. V.; Shalaev, V. M. Optical Cloaking with Metamaterials. *Nat. Photon.* **2007** *1*, 224–227.

16. Pendry, J. B.; Martin-Moreno, L.; Garcia-Vidal, F. J. Mimicking Surface Plasmons with Structured Surfaces. *Science* **2004**, *305*, 847–848.

17. Garcia-Vidal, F. J.; Martin-Moreno, L.; Pendry, J. B. Surface with Holes in Them: New Plasmonic Metamaterials. *J. Opt. A, Pure Appl. Opt.* **2005**, *7*, S97–S101.

18. Hibbins, A. P.; Evans, B. R.; Sambles, J. R. Experimental Verification of Designer Surface Plasmons. *Science* **2005**, *308*, 670–672.

19. Lockyear, M. J.; Hlbbins, A. P.; Sambles, J. R. Microwave Surface-Plasmon-Like Modes on Thin Metamaterials. *Phys. Rev. Lett.* **2009**, *102*, 073901.

20. Maier, S. A.; Andrews, S. R.; Martin-Moreno, L.; Garcia-Vidal, F. J. Terahertz Surface Plasmon-Polariton Propagation and Focusing on Periodically Corrugated Metal Wires. *Phys. Rev. Lett.* **2006**, *97*, 176805.

21. Williams, C. R.; Andrews, S. R.; Maier, S. A.; Fernandez-Dominguez, A. I.; martin-Moreno, L.; Garcia-Vidal, F. J. Highly Confined Guiding of Terahertz Surface Plasmon Polaritons on Structured Metal Surfaces. *Nat. Photon.* **2008**, *2*, 175–179.

22. Gan, Q.; Fu, Z.; Ding, Y. J.; Bartoli, F. J. Ultrawide-Bandwidth Slow-Light System Based on THz Plasmonic Graded Metallic Grating Structures. *Phys. Rev. Lett.* **2008**, *100*, 256803.

23. Elston, S. J.; Bryan-Brown, G. P.; Sambles, J. R. Polarization Conversion from Diffraction Gratings. *Phys. Rev. B* **1991**, *44*, 6393–6400.

24. Takano, T.; Hamasaki, J. Propagating Modes of a Metal-Clad-Dielectric-Slab Waveguide for Integrated Optics. *IEEE J. Quantum Elec.* **1972**, *8*, 206–212.

25. Moharam, M. G.; Gaylord, T. K. Rigorous Coupled-Wave Analysis of Planar-Grating Diffraction. *J. Opt. Soc. A* **1981**, *71*, 811–818.

26. Palik, E. D. *Handbook of Optical Constants of Solids*; Academic Press: New York, 1985.

27. Lee, K. G.; Park, Q. H. Coupling of Surface Plasmon Polaritons and Light in Metallic Nanoslits. *Phys. Rev. Lett.* **2005**, *95*, 103902.

28. Hsu, S. Y.; Lee, K. L.; Lin, E. H.; Lee, M. C.; Wei, P. K. Giant Birefringence Induced by Plasmonic Nanoslit Arrays. *Appl. Phys. Lett.* **2009**, *95*, 013105.

29. Xu, F.; Tyan, R. C.; Sun, P. C.; Fainman, Y.; Cheng, C. C.; Scherer, A. Fabrication, Modeling, and Characterization of Form-Birefringent Nanostructures. *Opt. Lett.* **1995**, *20*, 2457–2459.

30. Passilly, N; Ventola, K; Karvinen, P; Laakkonen, P; Turunen, J; Tervo, J. Polarization Conversion in Conical Diffraction by Metallic and Dielectric Subwavelength Gratings. *Appl. Opt.* **2007**, *46*, 4258–4265.

31. Feng, L.; Liu, Z.; Lomakin, V.; Fainman, Y. Form-Birefringence Metal and Its Plasmonic Anisotropy. *Appl. Phys. Lett.* **2010**, *96*, 041112.

32. Pang, L.; Tetz, K. A.; Fainman, Y. Observation of the Splitting of Degenerate Surface Plasmon Polariton Modes in a Two-Dimensional Metallic Nanohole Array. *Appl. Phys. Lett.* **2007**, *90*, 111103.

33. Navarro-Cia, M; Beruete, M.; Agrafiotis, S.; Falcone, F.; Sorolla, M.; Maier, S. A. Broadband Spoof Plasmons and Subwavelength Electromagnetic Energy Confinement on Ultrathin Metafilms. *Opt. Express* **2009**, *17*, 18184–18195.

34. Beruete, M.; Aznabet, M.; Navarro-Cia, M.; El Mrabet, O.; Falcone, F.; Aknin, N.; Essaaidi, M.; Sorolla, M. Electroinductive Waves Role in Left-Handed Stacked Complementary Split Rings Resonators. *Opt. Express* **2009**, *17*, 1274–1281.

35. Gansel, J. K.; Thiel, M.; Rill, M. S.; Decker, M.; Bade, K.; Saile, V.; Freymann, G. V.; Linden, S.; Wegener, M. Gold Helix Photonic Metamaterial as Broadband Circular Polarizer. *Science* **2009**, *325*, 1513–1515.

36. Liu, N.; Guo, H.; Fu, L.; Kaiser, S.; Schweizer, H.; Giessen, H. Three-Dimensional Photonic Metamaterials at Optical Frequencies. *Nat. Mater.* **2008**, *7*, 31–37.